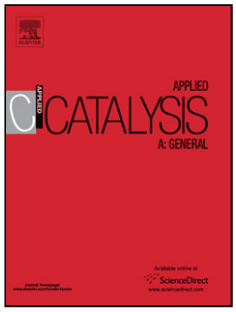

Title: Kinetics, thermodynamics and mechanisms for hydroprocessing of renewable oils

Author: Mohit Anand Saleem Akthar Farooqui Rakesh Kumar Rakesh Joshi Rohit Kumar Malayil Gopalan Sibi Hari Singh Anil Kumar Sinha

PII: S0926-860X(16)30103-X
DOI: http://dx.doi.org/doi:10.1016/j.apcata.2016.02.027
Reference: APCATA 15786

To appear in: *Applied Catalysis A: General*

Received date: 2-11-2015
Revised date: 24-2-2016
Accepted date: 25-2-2016

Please cite this article as: Mohit Anand, Saleem Akthar Farooqui, Rakesh Kumar, Rakesh Joshi, Rohit Kumar, Malayil Gopalan Sibi, Hari Singh, Anil Kumar Sinha, Kinetics, thermodynamics and mechanisms for hydroprocessing of renewable oils, Applied Catalysis A, General http://dx.doi.org/10.1016/j.apcata.2016.02.027

Kinetics, thermodynamics and mechanisms for hydroprocessing of renewable oils

Mohit Anand[1,2], Saleem Akthar Farooqui[1], Rakesh Kumar[1], Rakesh Joshi[1], Rohit Kumar[1], Malayil Gopalan Sibi[1], Hari Singh[1], Anil Kumar Sinha[1,2*]

[1]CSIR-Indian Institute of Petroleum, Dehradun-248 005, India; [2]Academy of Scientific and Innovative Research (AcSIR), CSIR-IIP, Dehradun-248 005, India, Fax: 91 135 2660202; Tel: 91 135 2525842; *E-mail: asinha@iip.res.in

Graphical abstract

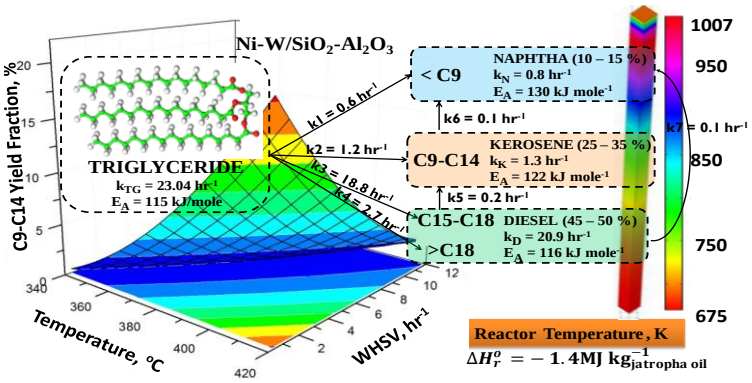

Highlights

- Hydroprocessing of triglycerides are not diffusion–limited over Ni-W/SiO_2-Al_2O_3
- Propane removal reaction was most exothermic, 85% of the total energy (1.34 MJ/kg)
- Highest exothermicity in top 1/5 (15-18%) of the catalyst bed due to depropanation

Abstract

Intrinsic kinetics, diffusivity, energy calculations and reaction mechanism studies for the conversion of plant-oil triglycerides over Ni-W/SiO_2-Al_2O_3 hydrocracking catalyst is reported. Specific insights into reaction mechanisms, are established using kinetic modeling and validated with experimental results. Diffusion studies and effectiveness factor calculations established diffusion–free intrinsic kinetics, with an activation energy of 115 kJ/mole required for triglycerides conversion. Thermodynamic calculations further established that the heat released during propane removal step (1.15 MJ/kg) was 8-times higher than that for hydrodeoxygenation step (0.14 MJ/kg) and lowest for hydrocracking reactions (0.08 MJ/kg). Such high exothermicity resulted in high temperature gradient across the catalyst bed (370°C above the reaction temperature).

Keywords: hydrocracking, triglyceride, biofuel, kinetics, thermodynamics.

1. Introduction

Renewable resources are the key to meet the growing energy needs of the world in a sustainable as well as environment friendly way [1-2]. In literature, hydroprocessing of various plant-derived oils like soybean oil, sunflower oil, jatropha oil, fresh and waste cooking oil, waste animal fats either directly [1-11] or via co–processing with gas oil [1, 2, 4, 5, 12-16] have been reported. Competitive reactions such as decarbonation (decarboxylation + decarbonylation) and hydrodeoxygenation along with various side reactions like water-gas shift and methanation reaction, and their effect on the main reactions for the conversion of vegetable oil into fuels, have been discussed [1, 2, 4, 13-14,

17-18]. Studies with model compounds and radioisotopic investigations have also been discussed for hydrodeoxygenation reaction pathways over various catalytic systems [19]. Effect of process parameters such as temperature, pressure, space velocity, and hydrogen-to-oil ratio on the various competitive reactions and on product patterns, during conversion of triglycerides [1, 2, 4, 8, 9 18-20] have also been discussed in prior literature. The shift in reaction mechanisms based on the changes in the concentration of various side products like carbon dioxide, carbon monoxide and water vapor have also been predicted [21]. As these reactions are highly exothermic with water as a reaction by-product, hydrothermal stability, catalyst life, along with regenerability and desired product patterns are key issues yet to be discussed in detail in the open literature, during the selection of the catalyst [1, 18, 22-23]. Very high exothermicity and hydrothermal conditions during reactions could have adverse affect on the catalyst which may collapse rapidly under these conditions, resulting in unpredictable or poor catalyst life.

Biomass derived oils contains 20-30 % oxygen content and vegetable oils which predominantly contain triglyceride molecules contain about 9-11 wt% oxygen, which is undesirable for hydrocarbon based transportation fuels. Unwanted waxy (oligomeric) oxygenated product formation is also reported during hydrotreating of these oxygenated feeds [22]. These unwanted oxygenated compounds not only tend to choke the catalyst bed, but also act as precursors for coke, and deactivate the catalyst. The enormous amount of oxygen (9-30%) in these feeds, as compared to sulphur based impurities present in conventional petroleum based feeds, necessitates severe hydrotreating with very strong hydrogenation/dehydrogenation functionality. Sulphided tungsten based catalytic systems (Ni-W) offer enhanced hydrogenation ability [2] as compared to sulphided molybdenum based catalysts (CoMo, Ni-Mo). The stronger hydrogenation ability is expected to reduce the formation of waxy oxygenated species and lead to enhanced catalytic activity, with

increased catalyst life [2]. Hydrodesulphurization mechanisms, and intermediates formed during these reactions have been studied in detail [23]. Detailed studies on kinetics [22, 24] for hydrodeoxygenation of model compounds such as acrolein [25], tristerian (glycerol tristearate C18) [26], triolean (glucerol trioleate C18) [26], tricaprylin (octanoic acid triglyceride C8) [27], caprylic acid (octanoic acid C8) [27], stearic acid [28, 29] and oleic acid [19, 21, 30] etc. have also been reported to understand the reaction mechanisms for the conversion of these model compounds. Studies on diffusion [31-32], detailed kinetics, reaction pathways and thermodynamics, including energy barriers predictions for hydrodeoxygenation of real bio-based oxygenated feedstocks are yet to be reported over hydrocracking catalytic system. This work reports the diffusion limitations, kinetics, reaction mechanisms and thermodynamics for jatropha oil as an oxygenated renewable feed over Ni-W/SiO_2-Al_2O_3 catalyst in a fixed bed reactor.

2. Material and methods

Jatropha oil (1.7% FFA (free fatty acids), 19.5% C16:0, 7.9% C18:0, 45.4% C18:1, 27.3% C18:2, 77.0 wt% C, 13.6 wt.% H, 9.4 wt.% O, 4.0 ppm S; Na: 3.2, K: 28.9, Mg: 17.3, Ca: 21.5, P: 35.6, Si: 6.4 ppmw), containing mainly triglycerides of C16 and C18 hydrocarbons was used as a feed for catalytic evaluations (Table 1). The catalyst was prepared by incipient-wetness impregnation method using nickel nitrate (Sigma-Aldrich) and tungsten chloride (Sigma-Aldrich) salts, over commercial extrudates of mesoporous SiO_2-Al_2O_3 support (Sasol). The catalyst was characterized for physico-chemical properties (SI Experimental details). Brönsted and Lewis acid sites of the catalyst sample were determined by DRIFTS (Diffuse Reflectance Fourier Transform Infrared Spectroscopy) using pyridine as a probe molecule (SI Experimental details) [33]. The feed and products were analyzed

using various analytical tools (SI Experimental details). For kinetic model development (lumped kinetic models) [22, 24, 34], <C9 carbon range liquid products were grouped as naphtha, C9-C14 carbon range products were grouped as kerosene and >C15 products were grouped as diesel. Isothermal microreactor was used for the kinetic models, with negligible variation in T across the catalyst bed (ΔT of $\pm$ 2^{o}C). The isothermal conditions were assured in the reactors with three zone furnace (ATS make) for micro reactors and five zone furnace (ATS make) for pilot scale reactor, which were maintained at the reaction temperatures using auto tuned controllers. The isothermal conditions were assured (for the microreactor) by three control thermocouples touching the reactor wall (horizontally passing through the furnace) and a response thermocouple kept at the heart of the catalyst bed. To assure isothermal conditions in the pilot scale reactor three response thermocouples were placed vertically across the catalyst bed to verify the isothermal conditions (Figure S1). And five control thermocouples were outside the reactor touching the reactor walls (passing through the furnace horizontally) (Figure S1). Continuous temperature monitoring was done with temperature variation of $\pm$ 2 ^{o}C. Details of experimental fitting of these models and energy barrier predictions [35] are given in supplementary information. The product patterns obtained on pilot scale were used for heat of reaction calculations (SI Experimental details). The experiments were carried in automated fixed bed micro-reactor (Hi-Tech Engineering Inc, Pune, India) and pilot scale reactor (Xytel India Ltd, Pune, India) with multi zone furnace in continuous down-flow mode. Hydrogen pressure was controlled by a back pressure regulator (TESCOM), gas flow was controlled by a mass flow controller (Brooks), and temperatures of the catalyst bed were controlled by temperature controllers and registered by thermocouples. A high pressure liquid metering pump (Eldex) was used to maintain desired liquid flow. The gas-liquid reaction effluent mixture passed through the gas-liquid separator to separate gaseous fractions from liquid hydroprocessed effluent. The

gaseous products were analysed online using a refinery gas analyser (RGA) details in SI experimental details. Material balance and atomic balance were performed to remove any error in experimental measurements. All reaction products were withdrawn after stabilization (8-12 hrs) of reaction conditions in each experiment and were analyzed once during the stabilization period and twice after the stabilization (product collection) by gas chromatography (GC) to confirm constant activity. A variation of ± 2.5 % in yields was considered as experimental measurement error. The yield of liquid products was calculated on a relative basis considering the entire range of products formed as 100 %. The extent of each reaction and individual heats of reactions were used to calculate the overall heat of reaction for the conversion of jatropha over NiW/SiO_2-Al_2O_3 catalyst.

Diffusivity and effectiveness factor were evaluated for kinetics calculations. Effective diffusivities of the reactant and product component lumps were calculated using bulk (D_{AB}) and Knudsen (D_{KA}) diffusivities (eq 1.). The bulk diffusion of the reactant species into the catalyst external surface was calculated using Stokes-Einstein relation (eq. 2). Diffusion of reacting species into the pores (the catalyst internal surface) was calculated using Knudsen diffusivity given by eq. 3, at two different temperatures, 340 ^oC and 420 ^oC.

$$\frac{1}{D_{AE}} = \frac{1}{D_{KA}} + \frac{1}{D_{AB}} \qquad \text{Eq. 1}$$

$$D_{AB} = \frac{K_b * T}{6 * \pi * r_h * \mu} \qquad \text{Eq. 2}$$

$$D_{KA} = \frac{D_p}{3} * \sqrt{\frac{8 * T * R_g}{\pi * M_{wt}}} \qquad \text{Eq. 3}$$

Here K_b is Boltzmann constant (1.38 * 10^{-23} m^2 kg s^{-2} K^{-1}), T is temperature in K, r_h is reactant hydrodynamic radius [32], μ is viscosity in Pa.sec, D_p is pore diameter, R_g is gas constant and M_{wt} is the molecular weightt of the reactant. Wagner-Weisz-Wheeler modulus

M_w and Thiele modulus M_T were evaluated by eq. 4, for predicting whether the reactant had completely wetted the catalyst particle and was free from any diffusion resistance [31].

$$M_w = \frac{(L^2) * (k_{observed})}{D_{AE}} = {M_T}^2 * \xi \qquad \text{Eq. 4}$$

Here L is the characteristic size of the catalyst particle defined to calculate the effective distance penetrated by the reactant molecule into the catalyst internal surface; $k_{observed}$ is the rate constant of the reaction; D_{AE} is the effective diffusivity of the reactant into the catalyst; ξ is the effectiveness factor. Effectiveness factor ξ is defined as the ratio of rate with external mass transfer resistance to rate without any mass transfer resistance and its value is 1 when the kinetics measured is intrinsic.

Comsol multiphysics 5.0 software was used for evaluating the product patterns and temperature profiles across the catalyst bed. The axial temperature gradients inside the pilot scale reactor were measured. The reactor diameter used for computational as well as experimental studies was small compared to the bed length (3 cm diameter, Length(L)/Diameter = 15), so radial temperature gradient was not observed experimentally and hence was not considered in the computational studies. The calculated activation energies and rate constants were used as inputs for reactor modelling. Three-dimensional Eulerian computational fluid dynamics model was developed based on principles of fluid film flow, statistical hydrodynamics and relative permeability concept. The model was verified using experimental results, to check if they correlated well.

3. Result and Discussion

3.1 Catalyst characterization

Processing plant oils such as those of jatropha over hydrocracking catalytic system like Ni-W/SiO_2-Al_2O_3 leads not only to deoxygenation reactions but also cracking and isomerisation reactions to form lower range hydrocarbons. The acidic SiO_2-Al_2O_3 support along with strong hydrogenation/dehydrogenation activity of sulfided metals (Ni-W), increases the cracking and isomerisation selectivity of the products [1, 4]. The total catalyst acidity as found by NH_3-TPD (100–650 ˚C) was 1.1 mmol/g (Figure S2a). The weak acid sites concentration (between 100-330 ºC) was 0.71 mmoles/$g_{catalyst}$, where as the strong acid sites concentration (between 330-650 ºC) was 0.38 mmoles/$g_{catalyst}$. DRIFT spectrum using pyridine as a probe molecule (Figure S2b) showed strong absorbance bands at 1545 cm^{-1} and 1500 cm^{-1} corresponding to Brönsted (B) and interacting (Lewis+Brönsted) acid sites, respectively; with a weak band at 1455 cm^{-1} corresponding to Lewis (L) acidity. The L/B population ratio as calculated from DRIFT spectrum (Figure S2b) was 0.56, however the results from DRIFT spectrum are not strictly quantitative as these are heavily affected by errors caused due to non-repeatability in particle size and packing density between different samples [33, 36]. SEM image of the fresh catalyst (Figure S3a) shows globular and elongated particles with <5µm size. Si/Al ratio was found to be 0.4 from SEM-EDX analysis. N_2-Sorption analysis showed type IV isotherm typical for mesoporous materials with hysteresis loop observed for adsorption and desorption cycles (Figure S4). BET surface area and pore volume after impregnation of metals and was found to be 250 m^2/g and 0.29 ml/g respectively. BJH analysis (Inset Figure S4) showed narrow pore size distribution with mean pore size of 4.6 nm.

3.2 Catalytic Studies

3.2.1 Triglycerides conversion:

Table 2 gives the conversion of jatropha oil triglycerides at different reaction conditions. The conversion of triglycerides increased gradually with increase in temperature from 340 to 420 ^{o}C, at higher space velocities (6-12 hr^{-1}, Table 2a); whereas at lower space velocities (0.5-3 hr^{-1}), complete conversion was observed at 360 ^{o}C and higher temperatures. The conversion increased rapidly with increasing temperature (1 hr^{-1}). Similar results were also observed earlier, with nearly complete conversions at 1-1.5 hr^{-1} space velocity and >360 ^{o}C temperatures over jatropha, soyabean, sunflower and algal oil lipids over different catalytic systems [1, 4, 8, 22 37, 38]. Pressure variation was found to have immense effect on the triglyceride conversion when all other reaction parameters (temperature, space velocity, H_2/feed ratio) were constant. Complete conversion of triglycerides could be achieved only at higher pressures (>60 bar) (Table 2b). At 420 ^{o}C (80 bar, 3 hr^{-1}) little effect of H_2/feed ratio on conversion was observed. Complete conversions were observed at H_2/feed ratios >500 Nl/L (Table 2c), whereas at lower temperatures 360 ^{o}C, the conversion gradually increased (47%) on increasing the ratio from 500 to 2500 Nl/L.

3.2.2 Product Yields:

At lower residence time (9, 6 hr^{-1}) the yield of deoxygenated product (C15-C18 range hydrocarbons) increased on increasing temperatures from 340-420 ^{o}C, due to increased conversion of triglycerides (Figure S5a and S5b), whereas at higher residence time (3, 1 hr^{-1}) there was an increase in formation of C15-C18 products observed till 370 ^{o}C, which was reduced on further increasing temperature (>370 ^{o}C) (Figure S5c and S5d). Enhanced formation of naphtha (<C9) and kerosene (C9-C14) fractions at lower space velocities (1 hr^{-1}) and higher temperatures (420 ^{o}C) (<C9 12% and C9-C14 20 %) (Figure S5a-S5d), was

observed. Increased yield of lower range hydrocarbons (<C15) observed at higher temperatures (360 ^{o}C or greater) and 1-1.5 hr^{-1} space velocity for sunflower, soyabean, jatropha and reduction in C15-C18 yield, were very much similar to the product patterns over other catalytic systems [1, 8, 24]. The results indicate the need to operate at higher residence time and higher reaction temperatures to maximize the yield of kerosene.

A shift in reaction pathway from predominantly deoxygenation reactions at lower temperatures (≤ 360 ^{o}C) to simultaneous cracking, isomerisation and deoxygenation reactions at higher temperatures (>380 ^{o}C) is indicated by the increase in formation of cracked lower range hydrocarbons (<C9 and C9-C14) at higher temperatures, due to conversion of C15-C18 lump into smaller hydrocarbons at higher temperatures (Figure S5). Lumped kinetic models were developed (as discussed later) to understand the changes in reaction pathways with temperature and residence time.

3.2.3 Space Velocity Effect

Figure 1 shows the influence of space velocity on yield fractions of various product lumps and of unconverted triglycerides at 340 ^{o}C and 420 ^{o}C (80 bar, 1500 Nl/L). Conversion of the triglycerides decreased with increase in space velocity from 0.5 to 12 hr^{-1}, at all temperatures, 340-420 ^{o}C (Table 2a, Figure 1). Complete conversions were observed below 6 hr^{-1} at 420 ^{o}C, but only 73% conversion was observed even at 1 hr^{-1} at 340 ^{o}C. At 12 hr^{-1} 80% conversion was observed at 420 ^{o}C, whereas only 30% conversion was observed at 340 and 360 ^{o}C (Table 2a, Figure 1). In case of hydrotreating Co-Mo/Al_2O_3 catalyst 98% conversion of triglycerides was observed at 8 hr^{-1} and 360 ^{o}C temperature [22], whereas in the present study only 36% conversion could be observed at 9 hr^{-1} and 360 ^{o}C (66 % conversion at 6 hr^{-1}) over Ni-W/ SiO_2-Al_2O_3. The difference in catalytic activity for these systems may be due to different kinetics and intrinsic activity of these catalysts.

The theoretical product yield based on fatty acid compositions of the feedstock at 9 hr^{-1} and 360 ^{o}C temperature was calculated to be 7% for C16 and 29 % for C18 fatty acid conversion. The actual experimental yield for C15-C18 range products was found to be 29.4 % (9 hr^{-1} and 360 ^{o}C) which was less than the theoretical values obtained. Even at 6 hr^{-1} and 360 ^{o}C temperatures, similar results with experimental yields (51% for C15-C18) lower than the theoretical yields of 13% for C16 and 53% for C18 fatty acids conversion were observed. This difference in theoretical value and experimental value may be attributed to conversion of C16 and C18 fatty acids into oligomeric or lower range compounds at these conditions.

The yields of cracked products (<C9 and C9-C14 hydrocarbons) was very low and increased marginally on reducing the space velocity from (0.1% at 12 hr^{-1} to 0.3% at 0.5 hr^{-1}) at 340 ^{o}C (Figure 1a), whereas at higher temperatures (420 ^{o}C) a gradual increase in the yield of cracked products (<C9 and C9-C14 hydrocarbons) was observed on reducing the space velocity (from 6% at 12 hr^{-1} to 35% at 0.5 hr^{-1}) (Figure 1b). Similar increase in the yield of lower range cracked products (<C15) were also observed from the conversion of jatropha, soyabean, sunflower and waste cooking oil lipids over different sulfided hydrocracking catalytic systems [1, 5, 14, 37-38]. Increasing the reaction severity by increasing reaction temperature and residence time leads to increase in naphtha (<C9) and kerosene (C9-C14) product yields.

At lower temperature 340 ^{o}C (Figure 1a), there was an increase in formation of >C18 fraction on increasing the space velocity from 1 hr^{-1} (10% yield) to 12 hr^{-1} (25% yield), whereas at higher temperatures, 400 ^{o}C (Figure S6) and 420 ^{o}C (Figure 1b) a constant yield of this fraction (10-12%) was observed. Huber *et al.*(2007) and Anand *et al.,* (2012) also reported formation of waxy oxygenated species on reducing the reaction severity, i.e. by reducing temperatures or increasing the space velocity. These products were responsible for

choking of the reactor and deactivation of the catalyst [14, 22, 24]. On the contrary, the deoxygenated diesel range product (C15-C18 hydrocarbons) decreased on increasing the space velocity from 0.5 to 12 hr^{-1}, at lower temperature (340 ^{o}C, Figure 1a). On increasing temperature to 420 ^{o}C, the yield of C15-C18 hydrocarbon products increased from 50% (0.5 hr^{-1}) to 78% (6 hr^{-1}) and then further decreased to 62% (at 12 hr^{-1}) due to reduced residence time. The yield of diesel fraction (C15-C18 hydrocarbons) decreases at lower space velocities (<6 hr^{-1}) due to increase in cracking reactions leading to increased yield of <C9 and C9-C14 hydrocarbon fractions at 420 ^{o}C (Figure 1b). The maxima in the yield of C15-C18 products shifted from 3 hr^{-1} (at 400 ^{o}C, Figure S6) to 6 hr^{-1} (at 420 ^{o}C, Figure 1b), with increase in temperature. This shift in maxima is due to increased cracking of C15-C18 range hydrocarbon products at higher temperature (420 ^{o}C) as well as due to a change in pathway for the conversion of triglycerides (direct hydrocracking), which is discussed later by developing kinetic models assuming various pathways for reactions. The conversions and yield of products obtained indicated that the reactions over Ni-W/SiO_2-Al_2O_3 catalyst were kinetically controlled and were very strongly dependent on the residence time inside the reactor.

3.3 Pilot Scale Evaluation:

Extended pilot scale evaluation (480 hrs) of this catalytic system showed comparable catalytic performance with micro-reactor studies. Typical yields of various products were: 12% naphtha (<C9 hydrocarbons), 30% kerosene (C9-C14 hydrocarbons) and 60% diesel (>C14 hydrocarbons). Detailed hydrocarbon analysis for the product showed that it contained 72% paraffins, 21% cyclic hydrocarbons, 7% mono-aromatics and 0.1% polyaromatic hydrocarbons (Figure S7). The physiochemical properties of kerosene range products were monitored with time on stream. The product met all the specifications of ASTM D1655 for aviation kerosene Jet A-1 and ASTM D7566 for renewable Jet A-1

kerosene. As the product pattern and properties started to change with time, the catalyst was regenerated (after 480 hrs), to check the regenerability of the catalyst. The catalytic performance could be regained after in-situ regeneration in air (Table 3). The conversion and yield fraction of different products after regeneration was found to be similar to those obtained at the start of run after stable reaction conditions were achieved (Table 3).

3.4 Mass Balance

Atomic balance and overall material balance for the reactions was carried out to remove errors in experiments (Table S1). Atomic balance results correlate very well with the gas chromatographic results, for example, 10% of oxygen from total oxygen content in jatropha oil (along with 71% carbon) was retained in liquid organic phase product which corresponds to the 10% >C18 product observed at 420 ^{o}C, 1 hr^{-1}, 1500 Nl/L and 80 bar (Figure 1a). This implies that the remnant oxygen was present in the oligomeric (>C18 products). 29 % of carbon from jatropha oil was observed in the gas phase due to cracked lower range hydrocarbons at these conditions.

3.5 Reaction pathway and model validation

The reaction schemes and empirical lumped kinetic models framed in scheme 1 for the hydrocracking catalyst (Ni-W/SiO_2-Al_2O_3) were validated with the experimental results. These models were developed after observing reaction product patterns obtained over hydrocracking catalyst. All possible reaction pathways were considered (Models 1-8, Scheme 1). Statistical tests were used for analyzing the goodness of fit of the models. The models were evaluated at two extreme temperatures, i.e. lower (340 ^{o}C) and higher (420 ^{o}C).

The possibility for M2 and M6 model pathways at both the temperatures was ruled out because of negative values of rate parameters (Table S2). Based on these observations the

direct conversion of triglycerides into various hydrocarbons and internal secondary cracking reactions are ruled out. Also, M4 and M5 models were rejected because of large deviations from experimental data indicated by very high chi square (χ^2) values and negative R^2 values at both temperatures (Table S2), which rules out cracking of triglycerides into diesel and further cracking of diesel into lower hydrocarbons.

M6 model pathway instead considered >C18 product in diesel lump to be formed directly as a primary reaction product from triglycerides (which was acceptable), but also as a secondary reaction product from the C15-C18 deoxygenated lump in diesel pool, which was not in accordance with the stable appearance of >C18 products in our experiments. Similarly, rejection of M4 model pathway, which considered >C18 formation from C15-C18 was also justified with experimental results.

At lower temperatures (340 ^{o}C) formation of naphtha (<C9) and kerosene (C9-C14) fractions were reduced. It is also anticipated that at low temperatures these products were not formed directly as a primary product of the reaction. This anticipation was confirmed with negative values of rate constants in the M7 model (k2 at 340 ^{o}C) and in the M8 model (k1 and k2 at 340 ^{o}C) pathways (Table S2). Both M1 and M3 model did not predict any negative rate constant values, but due to lower Chi square value for M3 pathway (M1 (χ^2, **142.1**), M3 (χ^2, **133.3**)), indicating lower error in prediction of rate constants (Table S2), which was supported by experimental results, where in suppressed yields of cracking products (naphtha and kerosene fractions) indicates that they are products of secondary cracking and not from direct cracking of triglycerides. Thus, M3 model was chosen to be the best model for triglyceride conversion at 340 ^{o}C temperature (Table 4).

At higher temperatures (420 ^{o}C), there is a drastic increase in the yield of the cracked products (naphtha and kerosene) and decrease in diesel yield. This observation indicated a

shift in reaction pathway from only deoxygenation reactions at lower temperatures (340 ^{o}C) to hydrocracking reactions at higher temperatures (420 ^{o}C). Similar observation was also reported for Co-Mo/Al_2O_3 catalyst [22]. M7 (**χ^2 value of 9.3**) and M8 (**χ^2 value of 8.9**) model pathways clearly satisfied all the criteria for acceptance with 95% confidence level and 5 degree of freedom (χ^2 <11.1) for goodness of fit, amongst M1, M3, M7 and M8 pathways (Table S2b). M7 and M8 models were very similar, but M8 model pathway considered inclusion of naphtha formation from diesel range (C15-C18) products into the rate equations (rate constant k7). Addition of this parameter in M8 model reduced the overall error as well as the Chi square value (least **χ^2 value of 8.9** and close to 1 R^2 value (0.99)). Hence M8 model pathway without any constraints was chosen to be the best model predicting the concentration of reactants and products at 420 ^{o}C (Table 4). Increased conversion of diesel range products into kerosene range as compared to naphtha range products was reflected in rate constant values (k5 = 0.2 hr^{-1} and k7 = 0.1 hr^{-1} at 420 ^{o}C), which were also justified by experimental results discussed earlier. At 340 ^{o}C conversions were lower which was indicated by low values of rate constants (Table 4) for triglycerides conversion and products formation, as compared to those observed at 420 ^{o}C. At higher 420 ^{o}C temperature, rate constants for triglycerides conversion along with other products formation were 15-30 times higher than those obtained at lower temperature (340 ^{o}C).

Simulated curves for both M7 and M8 models along with the experimental results, at 420 ^{o}C are shown in figure 3. Experimental conversion results fitted well with the simulated curves both for M7 and M8 models. The simulated curves for various products (<C9, C9-C14, C15-C18, >C18) also fitted well with the experimental values as shown in figure 2b & c for M7 and M8 models, respectively. For the naphtha range products a better fit was obtained for M8 model than for M7 model which is expected in accordance with the earlier discussion on pathway prediction.

To summarize the model fitting (Table 4), the reaction mechanisms followed at different temperatures over Ni-W/SiO_2-Al_2O_3 catalyst were slightly different from those reported over Co-Mo/Al_2O_3 catalyst [22]. At lower temperature (340 ^oC), the pathways were similar, i.e. deoxygenation reactions leading to formation of diesel as primary product were favoured, with naphtha and kerosene observed as secondary reaction products from cracking of C15-C18 lump (Table 4). At higher temperature (420 ^oC), there was shift in the reaction mechanism from only deoxygenation reactions to simultaneous hydrocracking and deoxygenation reactions (Table 4) along with severe cracking of diesel range molecules into naphtha range (<C9) products. This was not observed in case of Co-Mo/Al_2O_3 catalyst, which may be attributed to its low acidity [22]. But in the present study over the acidic SiO_2-Al_2O_3 support, naphtha (<C9 hydrocarbons) and kerosene (C9-C14 hydrocarbons) were formed due to direct hydrocracking of triglycerides as well as through secondary hydrocracking of C15-C18 lump. In-addition, kerosene was also observed to crack into naphtha and lighter hydrocarbons.

3.6 Diffusivity and energy calculations

Effective diffusivity (D_{AE}) for the reactant molecules, i.e. triglycerides, diesel and kerosene were calculated using equations 1-3 at 340 ^oC and 420 ^oC temperature (Table 5). Triglycerides being bulkier molecules (hydrodynamic radius, r_h=1.4*E-9 m), had reduced diffusivity, as compared to diesel (r_h=4.1*E-10 m) and kerosene (r_h=2.4*E-10 m) molecules at both the temperatures. Both Knudsen and bulk diffusivity for all the reactant species increased with increase in temperature from 340 ^oC to 420 ^oC (Table 5). As Knudsen diffusivity is dependent on the catalyst pore diameter and the molecular weight of reactant species, the effect of increased hydrodynamic radius for bulkier triglycerides molecules could be more prominently observed in bulk diffusivity values where transport of species from bulk solution to catalyst external surface was considered (Table 5). Calculation of

hydrodynamic radius and viscosity of reactant [32, 39] and characteristics size of the catalyst particle [31] are given in table S3. The Wagner-Weisz-Wheeler modulus (M_w) was used to determine the effectiveness factor. M_w values for the reactants i.e. triglycerides, diesel and kerosene molecules are given in table 5. These values at both the temperatures (340 and 420 ^oC) were < 0.15 which confirms that the effectiveness factor ξ is close to 1 [31]. Effectiveness factor ξ is a measure of complete wetting of the catalyst particle with reactants, and if the reactants are in diffusion free region its value should be '1'. Wagner-Weisz-Wheeler modulus (M_w) and Thiele modulus (M_T) values (M_w< 0.15 and M_T< 0.4) for the reactant and product molecules indicated that they were in diffusion free region and the kinetics measured were intrinsic [31]. M_w and M_T value >4 indicates strong pore resistance regime due to the centre of the catalyst particles being unused and starved of reactants [34], which was not observed from our calculations.

Activation energies and frequency factors for various lumps were calculated using Arrhenius plot (Table S4) for the conversion of triglycerides over Ni-W catalyst system. It was observed that the activation energy value for the conversion of triglyceride molecules was very high, (115 kJ/mole) as compared to that calculated earlier, (26 kJ/mole) for Co-Mo/Al_2O_3 [22]. We had attributed the low activation energy (for Co-Mo catalyst) to the formation of undesirable oxygenated (such as long chain acids) products at lower temperature which are not formed in case of Ni-W/SiO_2-Al_2O_3. This difference indicated that both Ni-W/SiO_2-Al_2O_3 and Co-Mo/Al_2O_3 catalytic systems produced different reaction intermediates and products, with different molecular interactions (solid-liquid-gas interactions), for the conversion of triglycerides. Hydrocracking Ni-W catalyst system produced intermediates which required higher energies for conversion into products, which was also evident with only 73% conversion observed at 340 ^oC and 1 hr^{-1} (Table 2a). The activation energy for the hydrocracking of triglycerides was found to be very similar to that

for the heavy petroleum residues (115 kJ/mole), over a commercial hydrocracking catalyst [40].

The activation energy for the formation of diesel product (116 kJ/mole) was similar to that for the triglyceride conversion, whereas that for naphtha (130 kJ/mole) and kerosene (122 kJ/mole) was much higher. These values (Table S4) indicated that more energy was required for production of cracked (naphtha and kerosene) compounds.

Heat of reaction for the conversion of jatropha oil over hydrocracking Ni-W/SiO_2-Al_2O_3 catalyst was calculated using heats of formation of the products obtained from the conversion of jatropha oil. The reactions considered for calculations were depropanation (-C_3H_8), hydrodeoxygenation (-H_2O), decarboxylation (-CO_2), decarbonylation (-CO) and hydrocracking (Table 6; SI, Heat of reaction calculations). Heat of formation of jatropha oil was calculated using the net calorific value obtained experimentally using calorimeter (SI Heat of reaction calculation). Using the heat of formation of the jatropha oil (triglyceride) and considering the most plausible reactions, heat of individual reactions were determined (Table 6). The total heat of reaction for jatropha oil hydrocracking was calculated using Hess's law, using the extent of individual reactions and the amount of products formed (Table 6, SI Heat of reaction calculations).

It was observed that for every one kilogram of jatropha, the amount of energy generated was, 1.15 MJ (depropanation reactions), 0.14 MJ (hydrodeoxygenation), 0.08 (hydrocracking of $C_{18}H_{38}$ and $C_{17}H_{36}$), whereas only 0.03 MJ was consumed by decarboxylation reaction. Of all the reactions, depropanation of triglyceride liberated maximum energy (nearly 6 times more than all other reactions), which is expected to occur in the top part of the catalyst bed and led to high temperature gradients predicted at the top part (15-18%) of the catalyst bed (Figure 3). A total energy of 1.34 MJ per kg of jatropha oil

is produced over hydrocracking Ni-W/SiO_2-Al_2O_3 catalyst system, which is nearly 10 times higher than the energy produced during cracking of vacuum gas oil (0.130 MJ/kg) [41]. Such large exothermicity led to enormous increase in catalyst bed temperatures and heat is required to be removed from the reaction zone to prevent temperature runaway and catalyst sintering. Reactor modelling studies were used to predict temperature profiles across the length of the catalyst bed at 420 ^oC temperature, 1500 Nl/L H_2/feed ratio, 80 bar pressure and 0.5 hr^{-1} space velocity (Figure 3). Temperature gradients along the length of the catalyst bed indicated a maximum temperature of 737 ^oC (1010 K) achieved in the top part (15-18%) of the catalyst bed (Figure 3) due to huge exothermicity of the reaction with high temperature gradient of 340 ^oC across the catalysts bed. The variations in the temperatures calculated at different fractions of the catalyst bed (Figure 3), indicates the need of suitable means to maintain the reactor temperature, such as by using liquid/gas quench streams required in different amounts at different zones of the reactor. In the first 15-18% of the catalyst bed major quench is required to avoid temperature runaway of the reaction. For the rest 80% of the catalyst bed, lower quench may be sufficient.

Reactor modelling studies were used to predict concentration profiles across the length of the catalyst bed at 420 ^oC temperature, 1500 Nl/L H_2/feed ratio and 80 bar pressure (Figure S08). The concentration of triglycerides dropped along the length of the catalyst bed from initial concentration of 1023 mol/m^3 to $6.03*10^{-10}$ (0.5 hr^{-1}) and 147.99 (12 hr^{-1}) mol/m^3. The major conversion of triglycerides (80% (0.5 hr^{-1}) and 70% (12 hr^{-1})) was indicated at the top of the catalyst bed (15-18% of bed) at 420 ^oC with 99.9% (0.5 hr^{-1}) and 85% (12 hr^{-1}) conversion at the end of the catalyst bed. These simulated results correlate to the experimental conversions, 100% (1 hr^{-1}) and 80% (12 hr^{-1}), reported (Table 2c). Only an additional 15-20% conversion was achieved in the remaining 80% of the catalyst bed, indicating marginal effect of space velocity at 420 ^oC, which led to insignificant reactant

triglyceride concentration gradients across the catalyst bed. The concentration of naphtha, kerosene increased from 0 mol/m^3(inlet) to 142, 240 mol/m^3 (outlet) at 0.5 hr^{-1}, respectively, whereas for diesel it initially increased to 660 mol/m^3 and then decreased to 520 mol/m^3 at 0.5 hr^{-1}, indicating further conversion of diesel pool compounds into cracked (naphtha and kerosene) products. However at 12 hr^{-1} the outlet concentration for naphtha and kerosene was less, whereas it was higher (696 mol/m^3) for diesel range products, due to reduced cracking.

4. Conclusions

To summarise, we establish for the first time that: (1) kinetics of hydroprocessing of plant-oil triglycerides are not diffusion–limited; (2) propane removal reaction was most exothermic (85% of the total energy generated) which released 8-12 times more energy, than that for other reactions (hydrodeoxygenation and hydrocracking); (3) large amount of energy released during propane removal reaction resulted in highest exothermicity in top one-fifth (15-18%) part of the catalyst bed.

Acknowledgment

The authors thank ASD, CSIR-IIP for analytical services and T. Khan and P. Alam for technical support for catalytic evaluations. MGS acknowledges UGC, India for fellowship. This work was carried under 'CSC-117' program of CSIR, India.DST, India is acknowledged for partial research funding.

Supporting Information

Catalyst characterization along with experimental details, product patterns and analysis after hydroprocessing of jatropha oil is discussed. Kinetic model evaluation, material and energy balance calculation and diffusion parameter evaluation procedures are discussed in detail.

REFERENCES

[1] R. Kumar, B. S. Rana, R. Tiwari, D. Verma, R. Kumar, R. K. Joshi, M. O. Garg, A. K. Sinha, Green Chem. 12 (2010), 2232-2239.

[2] R. Tiwari, B. S. Rana, R. Kumar, D. Verma, R. Kumar, R. K. Joshi, M. O. Garg, A. K. Sinha, Catal. Commun. 12 (2011) 559-562

[3] Y. Liu, R. Sotelo-Boyas, K. Murata, T. Minowa, K. Sakanishil, Chem. Lett. 38 (2009) 552-553.

[4] D. Verma, R. Kumar, B. S. Rana, A. K. Sinha, Energy Environ. Sci. 4 (2011) 1667-1671.

[5] S. Bezergianni and A. Kalogianni, Bioresour. Technol. 100 (2009) 3927-3932.

[6] D. Kubička, J. Horáček, M. Setnička, R. Bulánek, A. Zukal, I. Kubičková, Appl. Catal. B-Environ. 145 (2014) 101–107.

[7] C. Kordulis, K. Bourikas, M. Gousi, E. Kordouli, A. Lycourghiotis, Appl. Catal. B-Environ. 181(2016) 156–196.

[8] M. Krar, S. Kovacs, D. Kallo, J. Hancsok, Bioresour. Technol. 101 (2010) 9287-9293.

[9] J. Hancsok, T. Kasza, S. Kovacs, P. Solymosi, A. Hollo, J. Cleaner Prod. 34 (2012) 76-81

[10] P. Baladincz, J. Hancsok, Chem. Eng. J. 282 (2015) 152-160.

[11] J. Hancsok, P. Baladincz, T. Kasza, S. Kovacs, C. Toth, Z. Varga, J. Biomed. Biotechnol. http://dx.doi.org/10.1155/2011/384184

[12] S. Bezergianni, A. Kalogianni, I. A. Vasalos, Bioresour. Technol. 100 (2009) 3036-3042.

[13] S. Melis, S. Mayo, B. Leliveld, Biofuels Technol. 1 (2009) 43-47

[14] G. W. Huber, P. O. Connor, A. Corma, Appl. Catal. A: Gen. 329 (2007) 120-129.

[15] J. Mikulec, J. Cvengroš, L. Joríková, M. Banič, A. Kleinová, J. Cleaner Prod. 18 (2010) 917-926.

[16] C. Toth, P. Baladincz, S. Kovacs, J. Hancsok, Clean Technol. Environ. Policy 13 (2011) 581-585.

[17] B. Donnis, R. G. Egeberg, P. Blom, K. G. Knudsen, Top. Catal. 52 (2009) 229-240.

[18] N. H. Michaelsen and R. Egeberg, Hydrocarbon Processing 2009, 41-44.

[19] T. Szarvas, Z. Eller, T. Kasza, T. Ollar, P. Tetenyi, J. Hancsok, Appl. Catal. B-Environ. 165 (2015) 245-252

[20] P. Nair, A. Bozzano, T. Kalnes, Hydrocarbon processing sep (2007) 67l.

[21] J. G. Immer and H. H. Lamb, Energy Fuels 24 (2010) 5291-5299.

[22] M. Anand and A. K. Sinha, Bioresour. Technol. 126 (2012) 148–155

[23] W. Qian, A. Ishihara, S. Ogawa, T. Kabe, J. Phys. Chem. 98 (1994) 907–911.

[24] A. K. Sinha, M. Anand, B. S. Rana, R. Kumar, S. A. Farooqui, M. G. Sibi, R. Kumar, R. K. Joshi, Catal. Surv. Asia 17 (2013) 1-13

[25] D. R. Moberg, T. J. Thibodeau, F. G. Amar, B. G. Frederick, J. Phys. Chem. C 114 (2010) 13782–13795

[26] T. Morgan, D. Grubb, ES. Jimenez, M. Crocker, Top. Catal. 53(2010) 820.

[27] L. Boda, G. Onyestyak, H. Solt, F. Lonyi, J. Valyon, A. Thernesz, Appl. Catal., A: Gen. 374 (2010) 158-169.

[28] S. Lestari, P. Maki-Arvela, H. Bernas, O. Simakova, R. Sjoholm, J. Beltramini, G. Q. M. Lu, J. Myllyoja, I. Simakova, D. Y. Murzin, Energy Fuels 23 (2009) 3842-3845.

[29] M. Snare, I. Kubickova, P. Maki-Arvela, K. Eranen, D. Y. Murzin, Ind. Eng. Chem. Res. 45(2006) 5708-5715.

[30] M. Ahmadi, A. Nambo, J. B. Jasinski, P.Ratnasamy, M. A. Carreon, Catal. Sci. Technol. 5 (2015) 380-388.

[31] O. Levenspiel, Chemical Reaction Engineering, third ed., John Wiley & Sons., 1999, Ch. 18, p 388

[32] W. McCabe, J. Smith and P. Harriott, Unit Operations of Chemical Engineering, seventh ed., McGraw Hills, 2004

[33] C. R. Reddy, Y. S. Bhat, G. Nagendrappa, B. S. J. Prakash, Catal. Today. 141 (2009) 157-160.

[34] F. Trejo and J. Ancheyta, Catal. Today. 109 (2005) 99-103.

[35] M. A. Callejas, M. T. Martinez, Energy Fuels 14 (2000) 1309-1313

[36] A. Platon, W. J. Thomson, Ind. Eng. Chem. Res. 42 (2003) 5988-5992

[37] J. Cheng, T. Li, R. Huang, J. Zhou, K. Cen, Bioresour. Technol. 158 (2014) 378-382

[38] D. Verma, B. S. Rana, R. Kumar, M.G. Sibi, A. K. Sinha, J. Appl. Catal. A-Gen. 490 (2015) 108–116.

[39] S. Shokri and S. Zarrinpashne, Petroleum and Coal 48 (2006) 27-33

[40] D. Bahzada, R. Maroufa, A. Marafia, S. Togawab, Pet. Sci. Technol. 26 (2008) 50-63

[41] A. Moghadassi, N. Amini, O. Fadavi, M. Bahmani, Pet. Sci. Technol. 1 (2011) 31-37

Figure

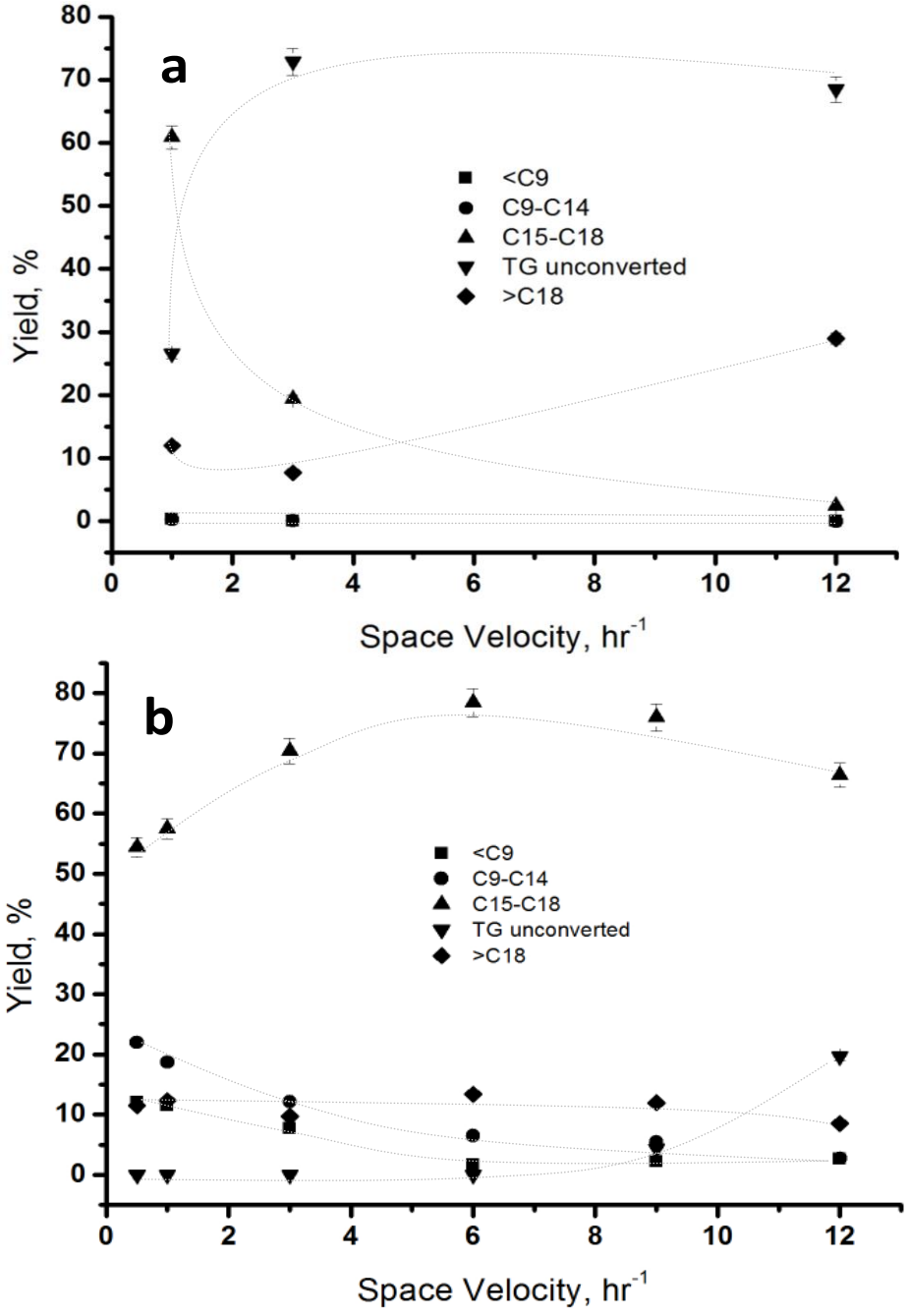

Figure 1. Influence of space velocity on yield fractions of various lumps ('TG' Triglycerides; 'Cn' hydrocarbons with carbon number 'n' (80 bar, 1500 Nl/L, a:340 ^{o}C; b:420 ^{o}C).

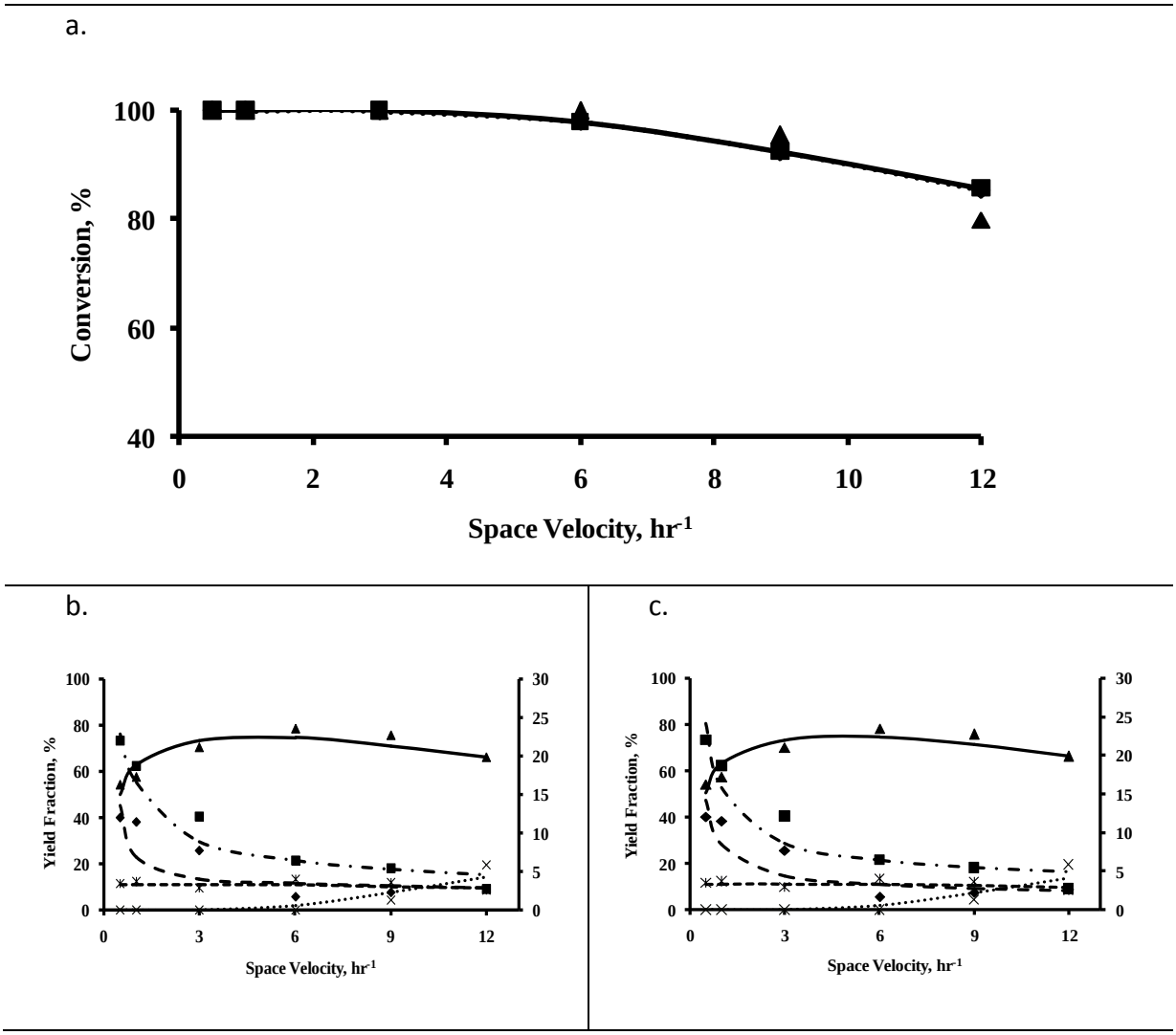

Figure 2. Fitting curves (420 ^{o}C, 1500 Nl/L, 80 bar) for experimental (▲) and model predicted (◆ M7, ■ M8) values of conversion (a.) and yield fraction (b. M7; c. M8) of products (◆ <C9, ■ C9-C14, ▲ C15-C18, × TG unconverted, ✳ >C18).

Temperature Gradients (K)		Bed Temperature Profile (C)
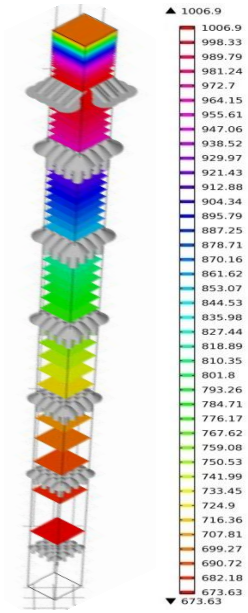	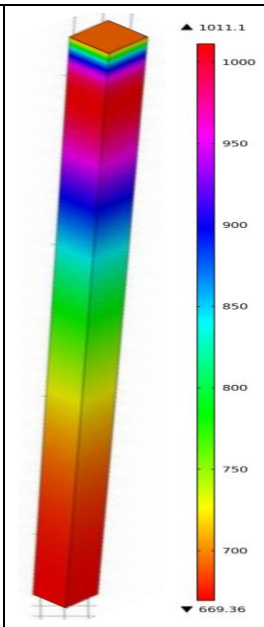	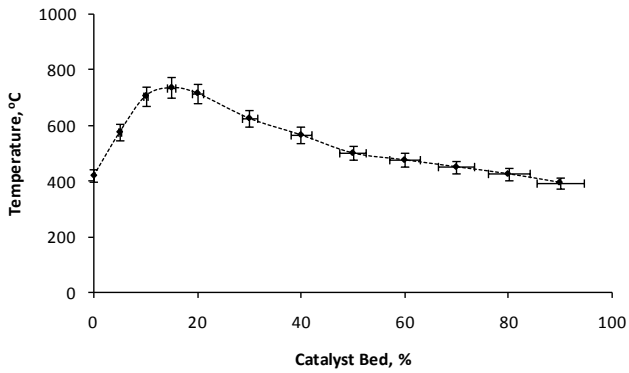

Figure 3. Temperature profile along the length of catalyst bed (420 ^{o}C, 1500 Nl/L, 80 bar, 0.5 hr^{-1})

Scheme 1. Reaction pathways for the conversion of triglycerides over Ni-W/SiO_2-Al_2O_3 catalyst system

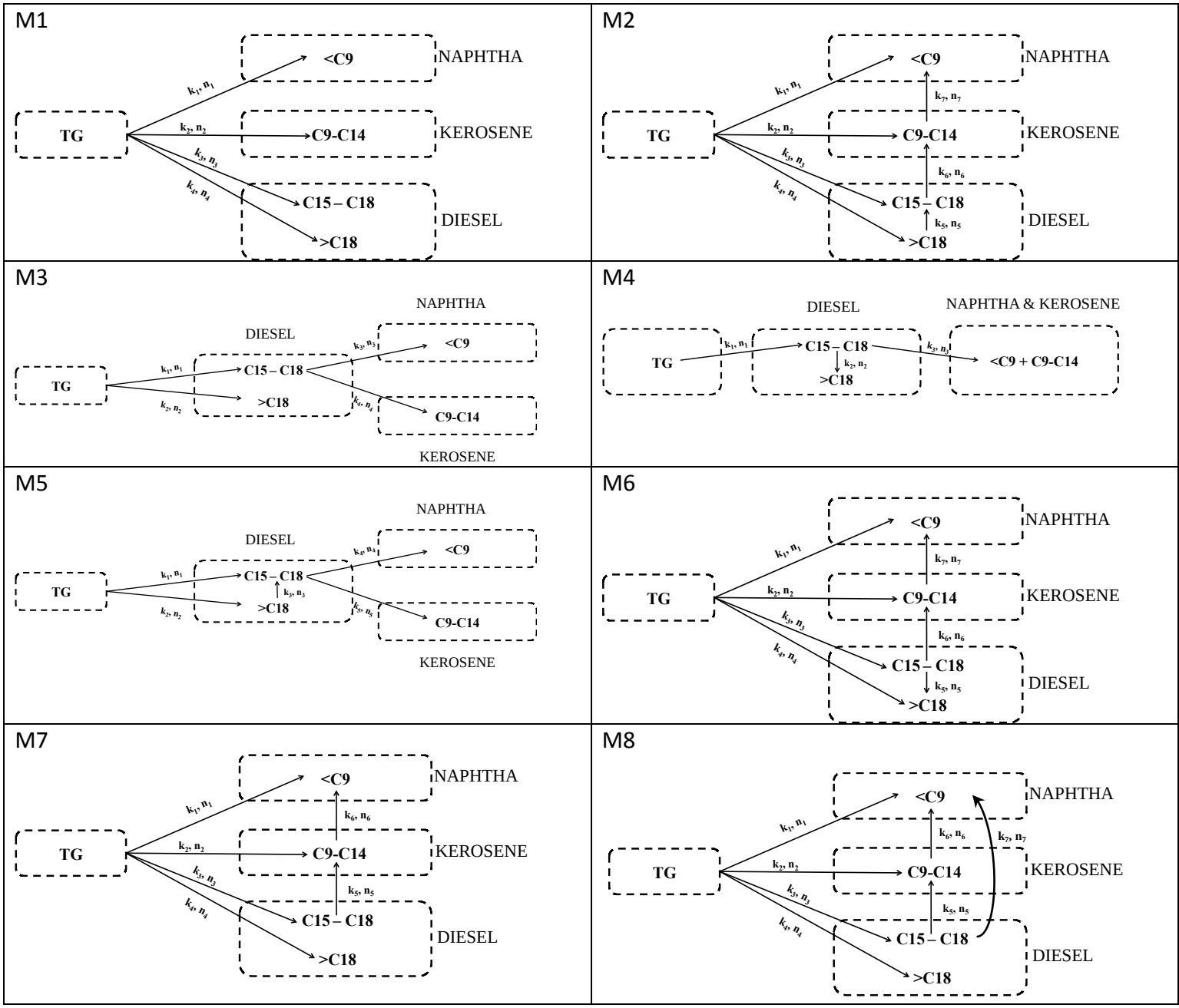

Tables

Table 1. Catalyst loading and processing conditions.

Catalyst	4% NiO, 24%WO_3, on SiO_2-Al_2O_3
Catalyst Mass, g	2 (microreactor), 100 (pilot-plant)
Catalyst Volume, ml	2.6 (microreactor), 150 (pilot-plant)
Catalyst shape	Powdered (microreactor), Extrudates (pilot-plant)
Bed length, cm	3.5 (microreactor), 45 (pilot-plant)
Bed Volume, ml	4.64 (microreactor), 318 (pilot-plant)
Reaction Temperature, ^oC	340 – 420
Reaction pressure, Bar	20 – 90
WHSV, hr^{-1}	0.5 – 12.0
H_2/feed, Nl/L	500-2500
H_2/feed, molar ratio	21.1-105.2

WHSV – Weight Hourly Space Velocity

Table 2. Conversion of triglycerides at various reaction conditions: a. Temperature effect (80 bar, 1500 Nl/L H_2/feed); b. Pressure effect (1500 Nl/L H_2/feed, 3 hr^{-1}, 420 ^oC); c. H_2/feed ratio effect (80 bar, 3 hr^{-1}).

a

Temp	Conversion, %					
^oC	0.5 hr^{-1}	1 hr^{-1}	3 hr^{-1}	6 hr^{-1}	9hr^{-1}	12 hr^{-1}
340		73		42	25	
360	100	100	100	66	36	29
400	100	100	100	85	51	29
420	100	100	100	100	96	80

b

Pressure, bar	Conversion, %
90	100
80	100
60	99.2
40	70.1
20	66.8

c

H_2/Feed,	Conversion, %	
Nl/L	360 ^oC	420 ^oC
2500	45.4	100
1500	39.0	100
1000	38.0	100
500	24.2	98.5

Table 3. Yield fractions of different products at different stages of pilot scale experimental runs at $1hr^{-1}$, 420 ^{o}C, 80 bar, 2500 Nl/L H_2/feed ratio (conversion, >99%).

Products	Start of Run	Before Regeneration	After Regeneration
Naphtha	12	3	13
Kerosene	30	22	32
Diesel	58	75	55

Table 4. Rate constants for accepted lumped models at 80 bar and 1500 Nl/L H_2/feed ratio.

Temperature, Kinetic Model	Rate Constant	Value, hr^{-1}	Error (±)
340 °C, M3	k' (Triglycerides)	1.06	0.27
	k1 (C15-C18)	0.85	0.17
	k2 (>C18)	0.20	0.10
	k3 (<C9)	0.04	0.11
	k4 (C9-C14)	0.04	0.11
420 °C, M8	k' (Triglycerides)	23.4	1.8
	k1 (<C9)	0.6	0.4
	k2 (C9-C14)	1.2	0.4
	k3 (C15-C18)	18.8	1.3
	k4 (>C18)	2.7	0.4
	k5 (C15-C18 cracking to C9-C14)	0.2	0.03
	k6 (C9-C14 cracking to <C9)	0.1	0.02
	k7 (C15-C18 cracking to <C9)	0.1	0.03

Table 5. Diffusivity, Wagner-Weisz-Wheeler (M_w) and Thiele (M_T) modulus for reactant molecules at various temperatures.

Temperature	Component	Diffusivity, m^2/sec			Modulus	
^oC		Knudsen, D_{KA}	Bulk, D_{AB}	Effective, D_{AE}	M_w	M_T
	Tiglycerides	1.8E-07	4.5E-10	4.5E-10	8.1E-04	2.8E-02
340	Diesel	3.5E-07	7.1E-09	7.0E-09	4.7E-05	6.9E-03
	Kerosene	4.6E-07	1.6E-08	1.5E-08	8.9E-07	9.4E-04
	Tiglycerides	2.0E-07	7.7E-10	7.7E-10	1.0E-02	1.0E-01
420	Diesel	3.7E-07	1.0E-08	9.9E-09	7.2E-04	2.7E-02
	Kerosene	4.9E-07	2.2E-08	2.1E-08	1.5E-05	3.9E-03

Table 6. Heats of reactions for the major reactions, during the hydroprocessing of jatropha oil.

Reaction $\Delta H_r^o = \sum \Delta H_{fProducts}^o - \sum \Delta H_{fReactants}^o$	ΔH_r^o, **MJ/mole**
Depropanation $C_{57}H_{110}O_6(v) + 3H_2(g) \xrightarrow{\Delta\ Catalyst} C_3H_8(g) + 3C_{18}H_{36}O_2(v)$	-1.02
Decarboxylation $C_{18}H_{36}O_2(v) \xrightarrow{\Delta\ Catalyst} CO_2(g) + C_{17}H_{36}(v)$	+0.03
Decarbonylation $C_{18}H_{36}O_2(v) + H_2(g) \xrightarrow{\Delta\ Catalyst} CO(g) + H_2O(v) + C_{17}H_{36}\ (v)$	+0.07
Hydrodeoxygenation $C_{18}H_{36}O_2(v) + 3H_2(g) \xrightarrow{\Delta\ Catalyst} C_{18}H_{38}(v) + 2H_2O(v)$	-0.079
Hydrocracking $C_{18}H_{38} + H_2 \xrightarrow{\Delta} C_{12}H_{26} + C_6H_{14} \quad \Delta H_{r\,C_{18}H_{38}}^o = -0.04247 MJ/mole$	-0.04
Hydrocracking $C_{17}H_{36} + H_2 \xrightarrow{\Delta} C_8H_{18} + C_9H_{20} \quad \Delta H_{r\,C_{17}H_{36}}^o = -0.043 MJ/mole$	-0.04